Supplementary Information

The use of N^N ligands as an alternative strategy for the sol-gel synthesis of visible-light activated titanias

Gamze Sarigul,[a, ±] Isabel Gómez-Palos,[b, ±] Noemi Linares,[a] Javier García-Martínez,[a] Rubén D. Costa,[b] Elena Serrano[a,*]

[a] Universidad de Alicante, Departamento de Química Inorgánica, Laboratorio de Nanotecnología Molecular, Ctra. San Vicente-Alicante s/n, E-03690 Alicante, Spain. www.nanomol.es
[b] IMDEA Materials Institute, Calle Eric Kandel 2, E-28906 Getafe, Madrid, Spain
[±] G.S. and I.G.-P. These authors contributed equally.
* elena.serrano@ua.es

TABLE OF CONTENTS

1. EXPERIMENTAL PROCEDURES

1.1 General methods

Structures of TBOT, Phen and the complex TBOT-Phen (Scheme 1 in the main paper) have been drawn and optimized using ACD/LABS2016.1.1 software, from ACDLabs. TiO$_2$(B,R)-Phen rutile and brookite structures were drawing starting from the CIFs corresponding to each of the structures (mp-2657 and mp-1840, respectively).

In order to determine the amount of phenanthroline incorporated into the titanias, thermogravimetric measurements (TG) were performed using a Mettler Toledo TG/SDTA analyzer under O$_2$:N$_2$ (1:4) atmosphere from room temperature to 900 ºC at a heating rate of 10 ºC min^{-1}. TG analysis of the materials before and after their use as photocatalysts was carried out using the same conditions and equipment.

IR spectra were recorded on a Nicolet Nexus FT-IR Spectrometer in a wavenumber range from 4000 to 500 cm^{-1}. Raman measurements were performed on a LabRam (Jobin-Ivon) raman dispersive spectrometer, 0.07 mW and using the excitation laser line at 632.8 nm.

X-ray Photoelectron Spectroscopy (XPS) was carried out in a VG-Microtech Multilab instrument, using MgK-alpha radiation of energy 1253.6 eV and pass energy of 50 eV. The analysis pressure during data acquisition was 5x10^{-7} Pa. A careful deconvolution of the spectra was made and the areas under the peaks were estimated by calculating the integral of each peak after subtracting a Shirley background and fitting the experimental peak to a combination of Lorentzian/Gaussian lines of 30-70 % proportions. Binding energies were referenced to the C1s line at 284.6 eV from adventitious carbon.[1]

The morphology of the synthesized materials was studied by transmission electron microscopy (TEM) using a JEOL JEM-1400 Plus instrument. Samples were suspended in ethanol and sonicated for 15 min. A few drops of this suspension were placed on a Lacey Formvar/Carbon copper grid. The ethanol was evaporated at room temperature. The digital analysis of the TEM micrographs was done using DigitalMicrographTM 3.6.1. by Gatan.

DRUV spectra were carried out in air at room temperature in the wavelength range 800-200 nm using a Shimadzu UV-2401 PC spectrophotometer with BaSO4 as the reference material. For the estimation of the band-gap, the reflectance data were converted into the equivalent absorption coefficient using the Kubelka-Munk formalism according to equation (1):

$$F(R') = \frac{[1-R']^2}{2R'}$$
(1)

where R' is the reflectance value obtained directly from the spectrophotometer. Band gap calculations are based on the $[F(R')h\nu]^{n/2}$ versus photon energy (hν) plot (Tauc plots).

The porous texture of the materials was characterized by N$_2$ adsorption/desorption isotherms at 77 K. Measurements were carried out in an AUTOSORB-6 apparatus. The samples were previously degassed for 8 h at 100 ºC at 5·10^{-5} bars. Specific surface areas were calculated using the BET method. Interparticle mesopore size was obtained by applying a NLDFT equilibrium model. Pore volume was directly read from the isotherms at a relative pressure of ca. 0.95.

1.2 X-ray diffraction experiments

Synchrotron X-ray diffraction experiments. Synchrotron experiments were performed on the power diffraction station of the BL04-MSPD beamline of the ALBA synchrotron located in the Barcelona area, Spain. Data were collected in transmission mode, at 20 keV, and using the position sensitive detector MYTHEN (beam size, 3 mm

horizontal, 0.7 mm vertical). Patterns were recorded in the 0.54 – 16.0 Å^{-1} Q-range, at the wavelength λ = 0.6197 Å, and then x-axis values were further converted to the CuKα radiation for plotting the data. Patterns were registered at room temperature, and with the sample filled in a 1.0-mm-diameter borosilicate capillary.

X-ray analysis. The phase content of any sample was calculated from the integrated intensities of the corresponding peaks, after subtraction of the X-ray patterns of the capillaries used in Synchrotron measurements and then, after baseline correction, using equations (2) to (4). The XRD patterns were fitted by using a Lorentz-Gaussian function. In the fitting it is assumed that peak broadening of brookite (120), (111), and (121) peaks are the same. Due to the overlap of the anatase (101) peak with the brookite (120) and (111) peaks, a numerical deconvolution technique was also used to separate these peaks when anatase phase was present in the samples.

$$w_A(\%) = \frac{K_A I_A}{K_A I_A + I_R + K_B I_B} \tag{2}$$

$$w_B(\%) = \frac{K_B I_B}{K_A I_A + I_R + K_B I_B} \tag{3}$$

$$w_R(\%) = \frac{I_R}{K_A I_A + I_R + K_B I_B} \tag{4}$$

where w_A, w_B and w_R are the weight fractions of anatase, brookite and rutile, respectively, and $I_{A(101)}$, $I_{B(121)}$ and $I_{R(110)}$ are the integrated intensities of the (101) anatase, (121) brookite and (110) rutile peaks in the XRD spectra, respectively. K_A = 0.886 and K_B = 2.721 are the correction coefficients optimized by Gribb and Banfield,[2] and Zhang and Banfield.[3]

The average crystallite size, referred to as domain size, was calculated by the Scherrer equation (5):

$$D = \frac{K\lambda}{\beta cos\theta} \tag{5}$$

where D is the average crystallite size (nm); λ is the wavelength of the radiation used (0.15406 nm for CuKα, K is the Scherrer constant (K = 0.93),[2] β is the full width at half maximum intensity, and θ is the angle associated to the main peak of each crystalline phase (these peaks are those at 2θ values of ca. 25.5, 27.6 and 31.0° for anatase, rutile and brookite, respectively). To calculate particle size, instrumental broadening was firstly determined from the (111) line of the commercial silicon standard measured in the synchrotron. Hence, the parameter β was calculated using the equation (6):

$$\beta = (FWHM^2 - b^2)^{1/2} \tag{6}$$

where b is the FWHM of the line (111) of the Si NIST standard.[3]

1.3 Photocatalytic experiments

The photocatalytic activity of TiO$_2$(B,R)-Phen materials was evaluated in the degradation reaction of representative cationic dyes in aqueous solution (Table S1), using a photochemical reactor system equipped with a 400 W medium-pressure Hg lamp (Photochemical Reactors LTD, UK) located in a cooled, double-walled quartz, immersion well (overall length 390 mm, internal diameter 38 mm, external diameter 58 mm, Model 3230, Photochemical Reactors LTD, UK). According to the supplier, this lamp produces predominantly 365-366nm radiation, with smaller amounts also in the ultraviolet region at 254, 265, 270, 289, 297, 302, 313 and 334 nm, and significant amounts in the visible region at 405-408, 436, 546 and 577-579 nm. Thus, a 2 M of freshly prepared NaNO$_2$ solution (liquid UV cut-off filter > 400 nm)[4,5] was introduced in the double-walled quartz immersion well, instead of distilled water, for each of the experiments conducted under visible irradiation. Transmittance spectra of the NaNO$_2$ solution was measured using a Jasco V-650 UV-vis spectrophotometer in the 200-800 nm range before each experiment to ensure the blocking

of the UV irradiation. The temperature of the dye solutions was kept between 30-35 °C in all the experiments by controlling the temperature of the circulating cooled $NaNO_2$ solution. The system is located inside a black photochemical safety reaction cabinet, and the photochemical reactor is fully covered by a heavy duty metal foil to wrap around the areas that emit radiation, Scheme S1. The light output, which was estimated using ferrioxalate actinometery[6–8] under these conditions (i.e. using the photochemical reactor system shown in Scheme S1 with the circulating cooled $NaNO_2$ solution), was 2.4 x 10^{16} photons/s.

Table S1. Name, abbreviation, chemical structure and wavelengths of maximum absorbance of the cationic (basic) dyes used in this work.

Cationic dye	Name	Abbreviation	Chemical structure	λ_{max} (nm)[1]
Rhodamine 6G	Basic Red 1	Rh6G		524.5
Methylene blue	Basic Blue 9	MB		661.5
Rhodamine B	Basic Violet 10	RhB		551.5
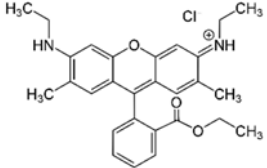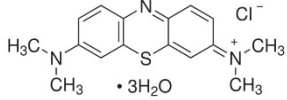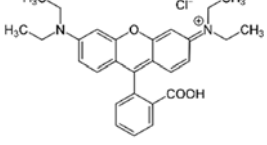
[1] Dye solutions (1 X 10^{-5} M) measured in a Jasco V-650 UV-vis spectrophotometer using quartz glass cells (optical path 10 mm), in the 200-800 nm range (scan speed: 1000 nm/min).
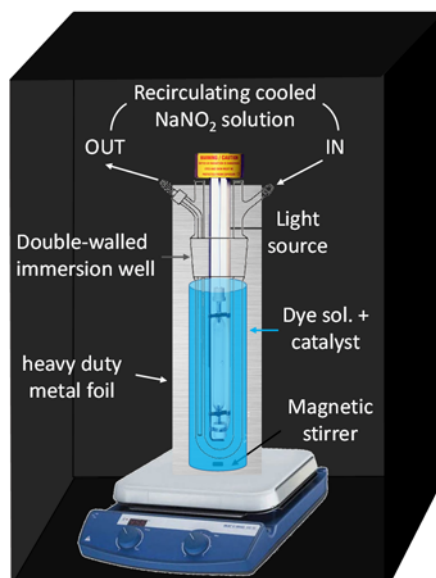
Scheme S1. Schematics of the photochemical reactor system used for the photocatalytic degradation tests, including a photograph of the double-walled quartz, immersion well and of the light source (see text for details).

Experiments were carried out using the reactor shown in Scheme S1, under identical irradiation conditions, keeping a photocatalysts concentration of 0.40 g L^{-1}, and using 100 ml of 1 x 10^{-5} M aqueous dye solutions, except for the

first series of experiments, in which the effect of the catalyst loading on the photocatalytic degradation reaction of Rh6G was assessed. This catalyst concentration, i.e. 0.40 g L^{-1}, is in line with the optimal concentration of the frequently employed titania powders having specific surface areas similar to the ones reported in this work.[9] A minimum of three runs for each system has been carried out in most cases to ensure reproducibility of the measurements. Statistics and error analysis have been included both in the main paper and in the additional results shown below. Two control experiments were carried out for each of the dye solution tested. The first one was carried out following the same procedure as described above, but without adding the solid to the photoreactor system. The second experiment was the running of the photocatalyst under dark (non-irradiating) conditions, no dye degradation took place, proving the photocatalytic nature of the synthesized TiO_2(B,R)-Phen.

Prior to each experiment, the suspension of the catalyst in the dye was stirred in dark a minimum of 60 min to achieve the adsorption/desorption equilibrium of the dye on the catalyst surface. To study adsorption of the dye in the dark, aliquots of samples were withdrawn every 15 min before the lamp was turned on, centrifuged at 4000 rpm for 10 min, and then the dye concentration was determined by UV-vis spectroscopy, using a Jasco V-650 UV-vis spectrophotometer in the 200-800 nm range (square cell with an optical path length of 10 mm, resolution 0.5 nm). In all cases, the initial concentration (C_0) has been taken as the concentration after the stirring in dark step, once the adsorption/desorption equilibrium was reached. The total concentration of Rh6G, RhB and MB species was estimated based on the maximum absorbance observed at ca. 525 nm, 550 nm and 660 nm, respectively, after baseline corrections (Table S1). High-pressure liquid chromatography–mass spectrometry (HPLC-MS) analysis of the dye solutions before after their bleaching was carried out in a gas chromatograph model Agilent 6890N equipped with a GERSTEL cis 4+(PTV) injector coupled to a mass spectrophotometer model Agilent 5973N. Some additional experiments were also carried out using an Aldrich® Micro Photochemical Reactor with blue LED lights as light source (435-445 nm spectral range), instead of the 400 W medium-pressure Hg lamp.

In a typical degradation test, an aqueous suspension of the dye ($1x10^{-5}$ M, 100 mL) with 0.40 g L^{-1} of as-synthesized photocatalyst was stirred in a 250 ml beaker, during 60 min in the dark, to achieve the adsorption/desorption equilibrium of the dye on the catalyst surface. Afterwards, the lamp was turned on and the suspension was irradiated using the photochemical reactor system shown in Scheme S1. Samples were then withdrawn every 5 - 20 min (depending of the system), centrifuged at 4000 rpm for 10 min, and then supernatant was analyzed using a Jasco V-650 UV-vis spectrophotometer in the 200-800 nm range (square cell with an optical path length of 10 mm, resolution 0.5 nm).

For comparison purposes, the photocatalytic activity of the Phen-free titania – sample TiO_2(A) –, of commercial P25 (Aeroxide P25, Across organics) as well as of the physical blend of TiO_2(A) with Phen (12 wt%) was also assessed in the degradation reaction of Rh6G ($1x10^{-5}$ M, 100 mL, 0.40 g L^{-1} of catalyst), under identical irradiation conditions.

Recycling tests. A total of four consecutive cycles were performed by the same batch of the synthesized TiO_2(B,R)-Phen photocatalyst, keeping a catalyst concentration of 0.4 g L^{-1} and a dye concentration (both Rh6G and MB) of $1x10^{-5}$ M. At the end of first cycle, the photocatalyst was recovered by centrifugation at 4000 rpm for 10 min, washed with water, centrifuged again at 4000 rpm for 10 min, and then air dried. This recovered solid was re-weighed and re-inserted into fresh Rh6G or MB solutions and irradiated with light as the second cycle. The same procedure was repeated for the third and fourth cycles of photocatalytic degradation.

Scavenger tests. Some experiments were also carried out using triethanolamine (TEOA, $1x10^{-2}$ M) as hole scavenger. The experimental procedure was similar to that described before, but adding the TEOA to aqueous dye solutions of Rh6G or MB before the photocatalytic tests, maintaining unchanged the other reaction conditions (catalyst concentration of 0.4 g L^{-1} and 100 ml of $1x10^{-5}$ M aqueous dye solutions).

In all cases, the plot of ln (C_0/C) vs irradiation time (t), where C_0 and C are the initial concentration (after achieving the adsorption/desorption equilibrium of the dye on the catalyst surface) and the concentration measured during the reaction, respectively, could be adjusted to a linear fit at low conversions, which means a pseudo-first reaction order. The photocatalytic constants (k') were thus estimated as the slope of those lineal fits, from the average of a minimum of three runs. The reproducibility of the constant rates is in the range of $\pm$ 10% in both Rh6G and MB degradation reactions.

After the degradation reactions, dye solutions were analyzed by HPLC/MS using an Agilent Model 1100 Series High Performance Liquid Chromatograph (HPLC) equipped with an electrospray ionization spray (EIS), coupled simultaneously to an Agilent 1100 Variable Wavelength UV-Visible Detector (254 and 600 nm) and a Mass Trap Spectrometer with Ion Trap Analyzer (Agilent Model 1100 Series LC / MSD Trap SL). The operating conditions were mass range m/z from 50 to 800 in positive mode, capillary 4kV, dry temperature 350 ºC, dry gas 12 l/min. The mobile phases used were A (water, 0.1% formic acid) and B (acetonitrile, 0.1% formic acid); the gradient program was as follows: 0–4 min 10–90% B, 4–8 min 90% B, 8–12 min 90–10% B, and 12–14 min 10% B, a flow rate of 1.0 ml/min, and an injection volume of 20 μL. The column used was a Poroshell 120 EC–C18 column (4.6 mm x 100 mm, 2.7 μm, ref. 695975-902, Agilent).

1.4 Measurements of electrochemical properties

TiO_2(A) and TiO_2(B,R)-Phen pastes were prepared adding 50 mg of the respective nanoparticles (TiO_2(A) or hybrid TiO_2(B,R)-Phen) in 200 μL of absolute Ethanol under stirring, after one hour, 50 μL of Hydrochloric acid 1M was added to the mixture. Pastes were stirred at room temperature overnight before their use. FTO substrates were sonicated for 15 min with a solution of Derquim® soap in water, rinsed with water and sonicated again with consecutive 15 min ultrasonic baths of water, and isopropanol and dried with nitrogen. After cleaning, they were treated in UV-O3 system for 18 min. The cleaned FTO were covered with an adhesive Scotch® tape with on the conductive side leaving a circular un-covered mask in the middle (6 mm diameter). Then a small amount of paste containing the semiconductor was placed on the tape near the inner mask. It was smoothened with a Doctor blade machine slider and the tape was removed. Electrodes were placed in an oven with air flow at 200 °C for 30 min.

For the counterelectrode fabrication, FTO substrates were drilled to create two small holes and then cleaned. A chloroplatinic solution (5 mM in isopropanol) was deposited dropwise on the conductive side and then heated at 450 °C for 20 min to create the Pt counter electrodes of the solar cells. The devices were assembled using a 25 μm thick Surlyn polymer placed around the active electrode separating it from the counter-electrode. To close it, the cell was pressed at 150 °C for 50 seconds melting the polymer. Afterwards, the electrolyte containing Iodide (0.03M), Guanidinium thiocyanate (0.10 M), 1-butyl-3-methylimidazolium iodide (0.6 M), 4-tert-butylpyridine (0.5 M) in an Acetonitrile/Valeronitrile mixture (85:15 %v), was injected through the pre-drilled holes in the CE. The holes were closed with a piece of tape to avoid evaporation. Finally, silver paste was used to paint contacts in both electrodes. To obtain the typical J-V current, the current is measured while applying increasing voltages under dark conditions and upon illumination. The sample is connected to a circuit and illuminated with a solar simulator (1 sun AM 1.5) through a 5 mm diameter mask. A potensiostat (Metrohm μAutolabIII) is used to monitor the photogenerated current at different applied voltages. Electrochemical impedance spectroscopic assays (EIS) were carried out with a potentiostat/galvanostat (Metrohm μAutolabIII) equipped with a frequency response analyzer module (FRA2). Measurements were performed at the applied voltage range from 0 to those of open circuit voltage for each device and fitted with the Nova software using the circuit model shown in Scheme 1. The AC signal amplitude was set to 15 mV, and modulated in a frequency range from 10 to 1 MHz. The charge transport resistance and resistance towards recombination are derived from assays under 1 sun illumination and dark conditions, respectively.
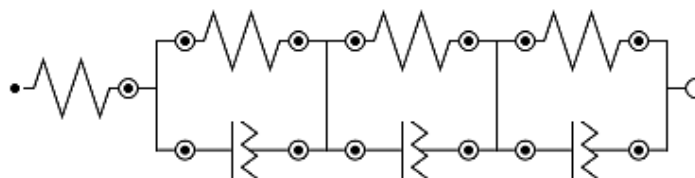
Scheme S2. Equivalent circuit for electrochemical cells prepared with the titanias. This consists in a series resistance representing external contacts, and three pseudo-capacitance/resistance elements in parallel, representing the interfaces within the cell, being electrode/electrolyte interface the dominant one.

2. ADDITIONAL RESULTS

2.1 Liquid NMR analyses
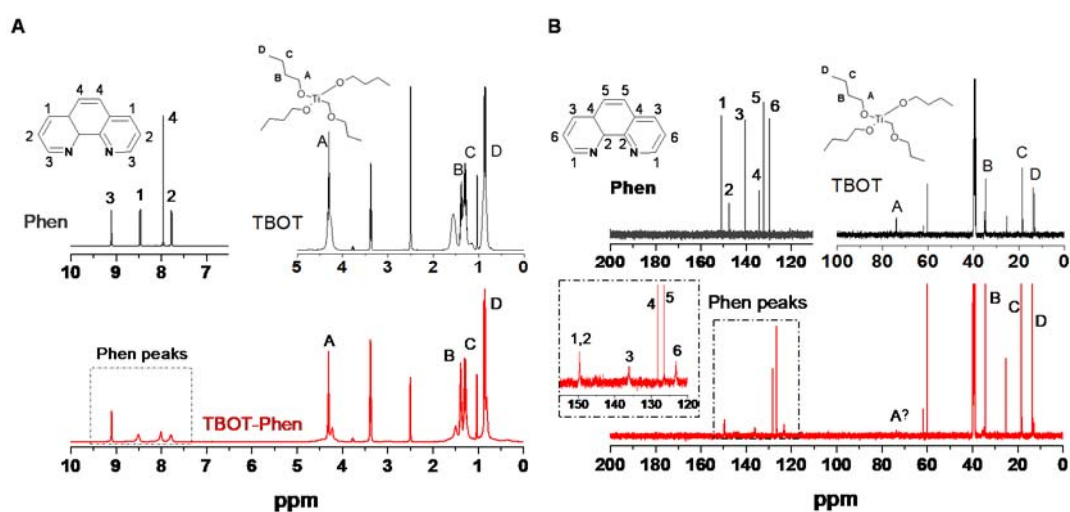
Figure S1. Liquid ^{13}C NMR **(A)** and ^{1}H NMR **(B)** spectra of the TBOT-Phen complex in deuterated DMSO, as compared with the spectra of the phenanthroline alone (Phen) and the TBOT.

2.2 XRD characterization
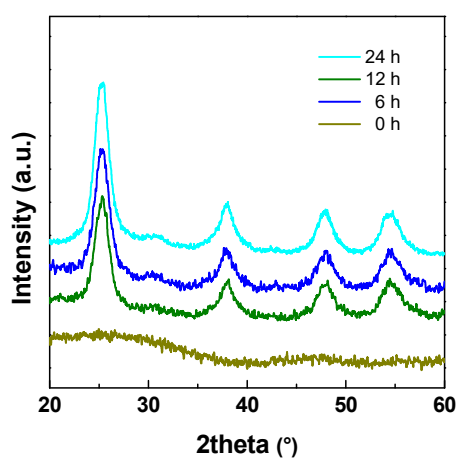
Figure S2. XRD patterns of the Phen-free titania –TiO$_2$(A) sample– as a function of the crystallization time at 80 ºC (adapted from ref.[10]).

2.3 XPS analyses
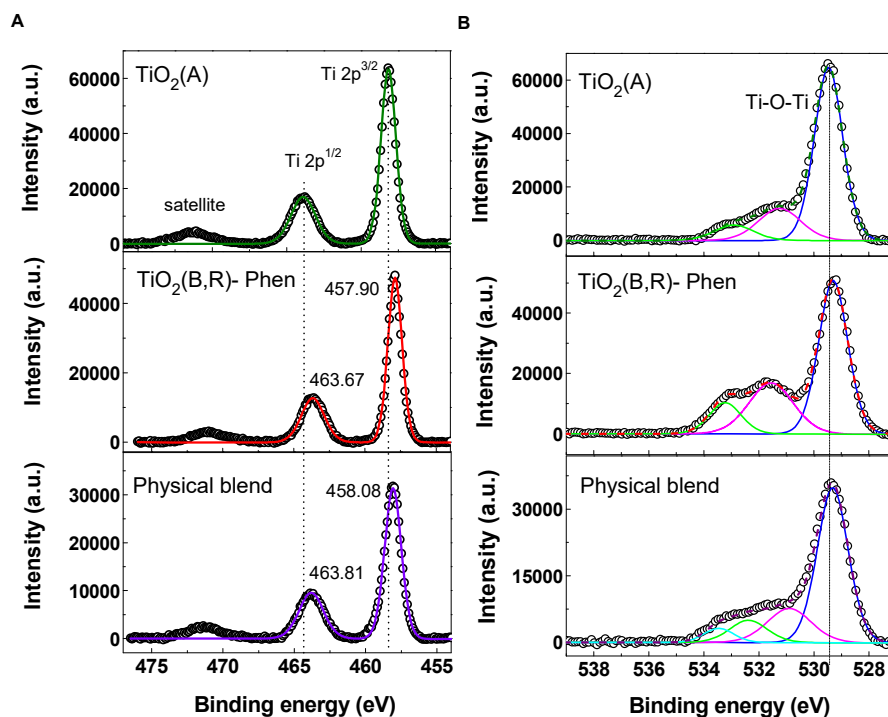
Figure S3. XPS spectra in the Ti 2p (**A**) and O 1s (**B**), regions of the hybrid TiO_2(B,R)-Phen (crystallization time 36 h) as compared with the unmodified TiO_2(A), and a physical blend of TiO_2(A) with 12 wt% Phen (physical blend). Points correspond to experimental data. The green/red/blue curves are the fitting of experimental data (black circles) for the different materials, which can be decomposed into a superposition of the different peaks (color lines).
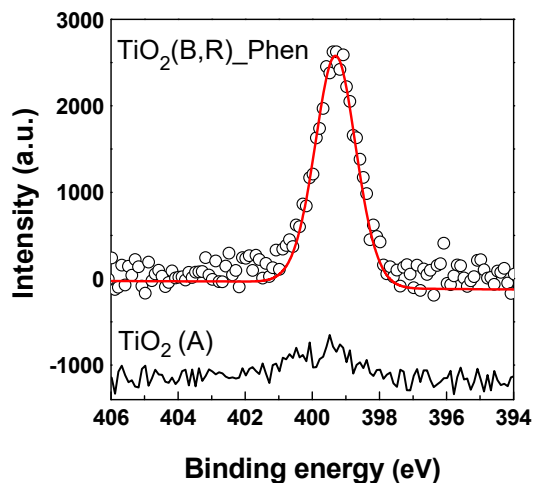
Figure S4. XPS spectra in the N1s region of the hybrid TiO_2(B,R)-Phen (crystallization time 36 h) as compared with the unmodified TiO_2(A). For the the hybrid TiO_2(B,R)-Phen, the red curve is the fitting of experimental data (black circles). Data for TiO_2(A) have been vertically shifted for the shake of clarity.

2.4 Synchrotron X-ray analyses
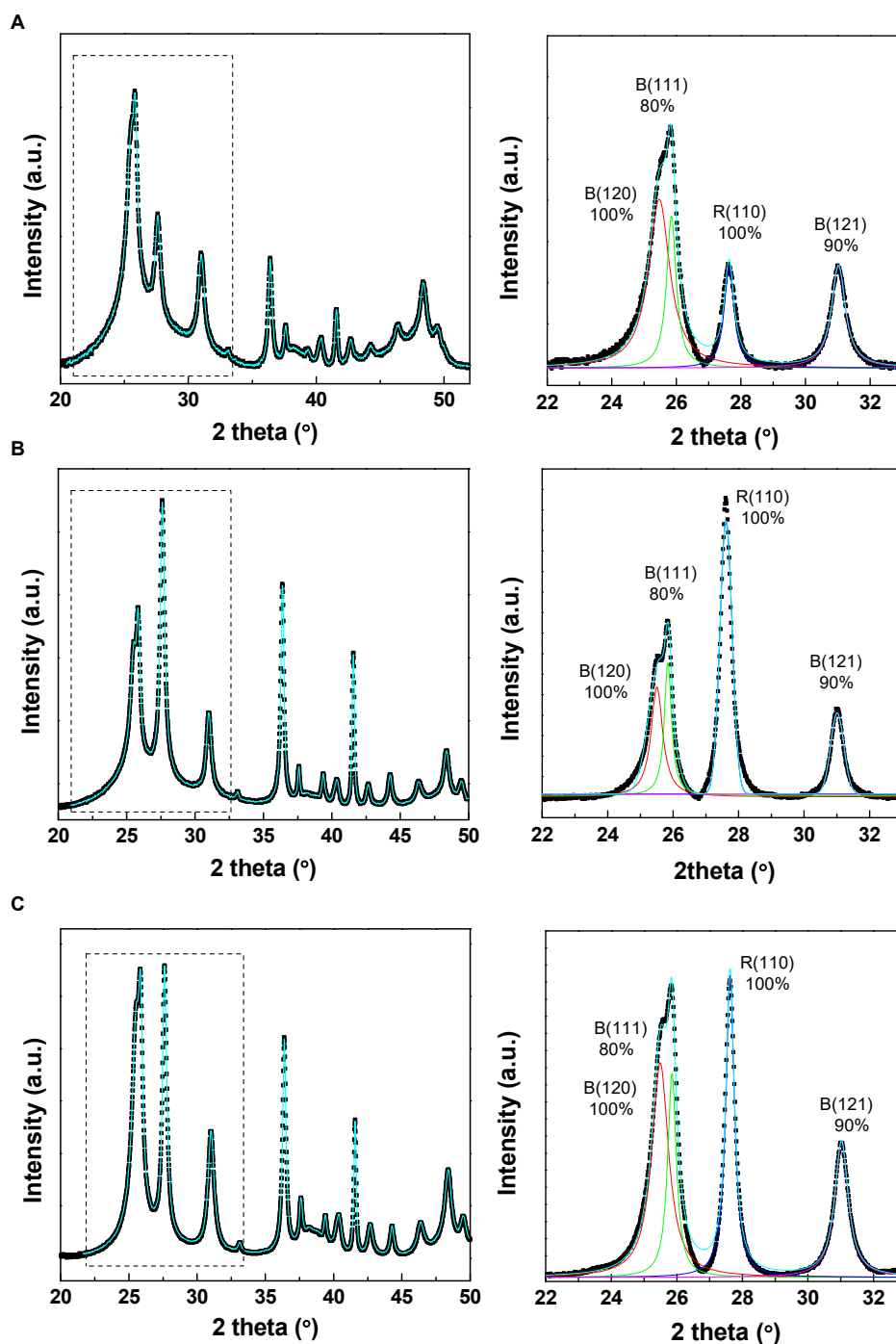
Figure S5. Deconvolution of synchrotron X-ray patterns of TiO$_2$(B,R)-Phen after: (**A**) 24 h, (**B**) 36 h, and (**C**) 48 h of crystallization at 100 ºC. Points correspond to experimental data.
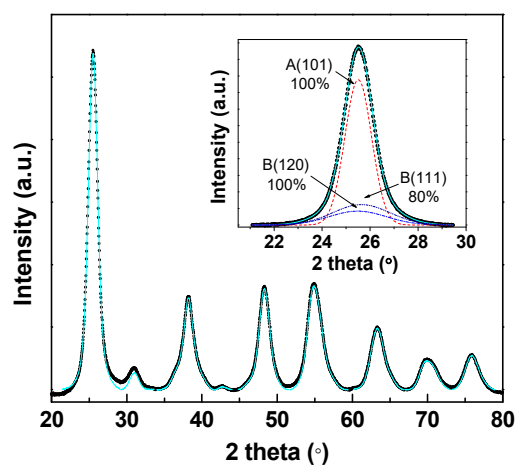
Figure S6. Deconvolution of synchrotron X-ray patterns of TiO$_2$(A) (crystallization time 36 h at 100 ºC). Points correspond to experimental data.
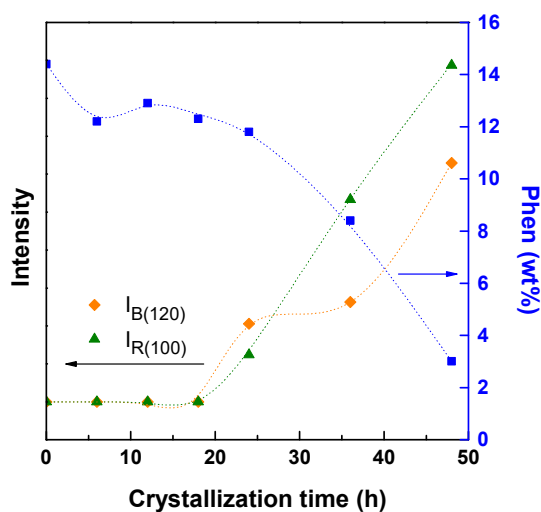
Figure S7. Evolution of the Phen incorporation, determined by TG, and the main crystallinity peaks of brookite and rutile in TiO$_2$(B,R)-Phen as a function of the crystallization time at 100 ºC. Dashed lines are interpolated to guide the eye.

2.5 Gas adsorption experiments
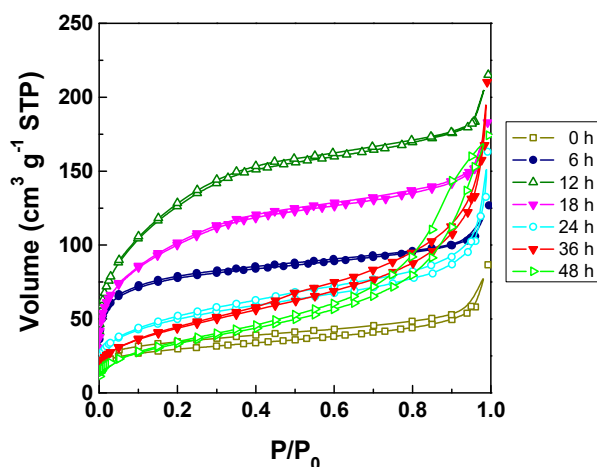
Figure S8. N_2 adsorption/desorption isotherms at 77 K of the hybrid TiO_2(B,R)-Phen as a function of the crystallization time at 100 ºC.

2.6 Photocatalytic activity characterization
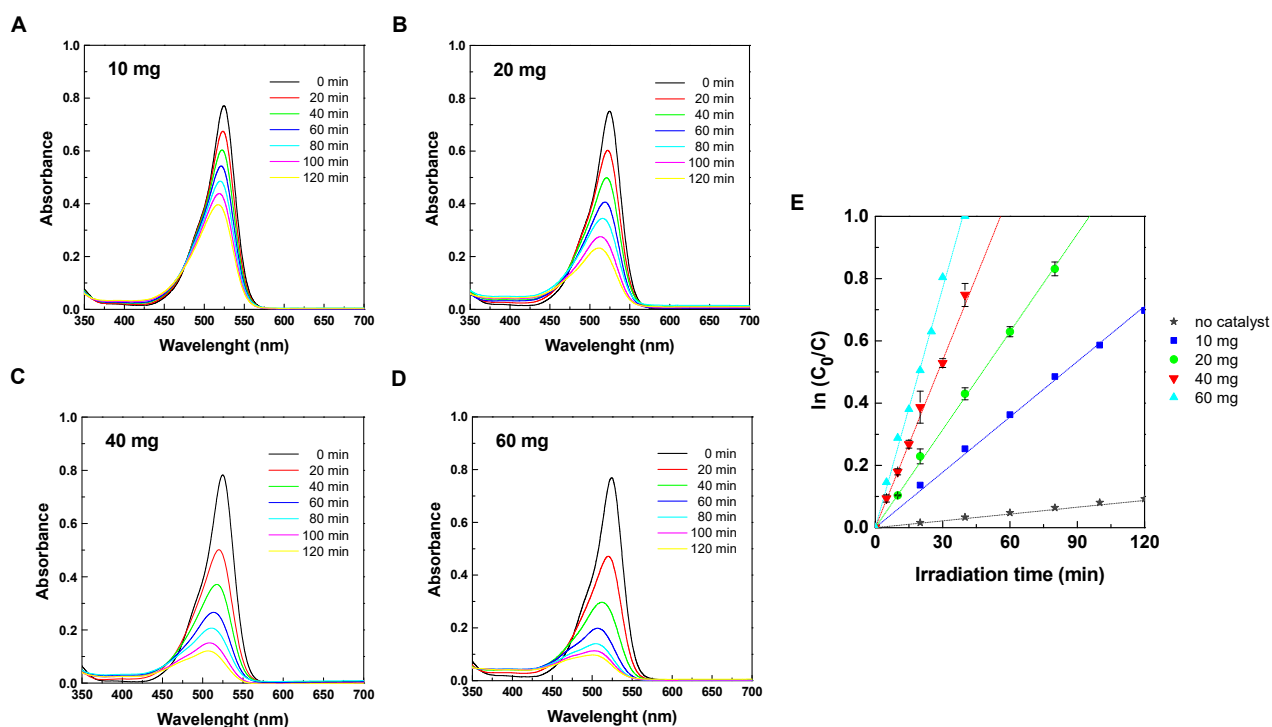
Figure S9. UV-vis absorption spectra of the degradation reaction of Rh6G under visible light irradiation using: (**A**) 10 mg, (**B**) 20 mg, (**C**) 40 mg, and (**D**) 60 mg of the hybrid TiO_2(B,R)-Phen (crystallization time 36 h) as photocatalyst. (**E**) Plots of ln (C_0/C) as a function of the irradiation time (symbols) and their corresponding linear fits (dashed lines) for each of the systems. Experiments were carried out under identical irradiation conditions, using 100 ml of 1 x 10^{-5} M aqueous Rh6G solutions.
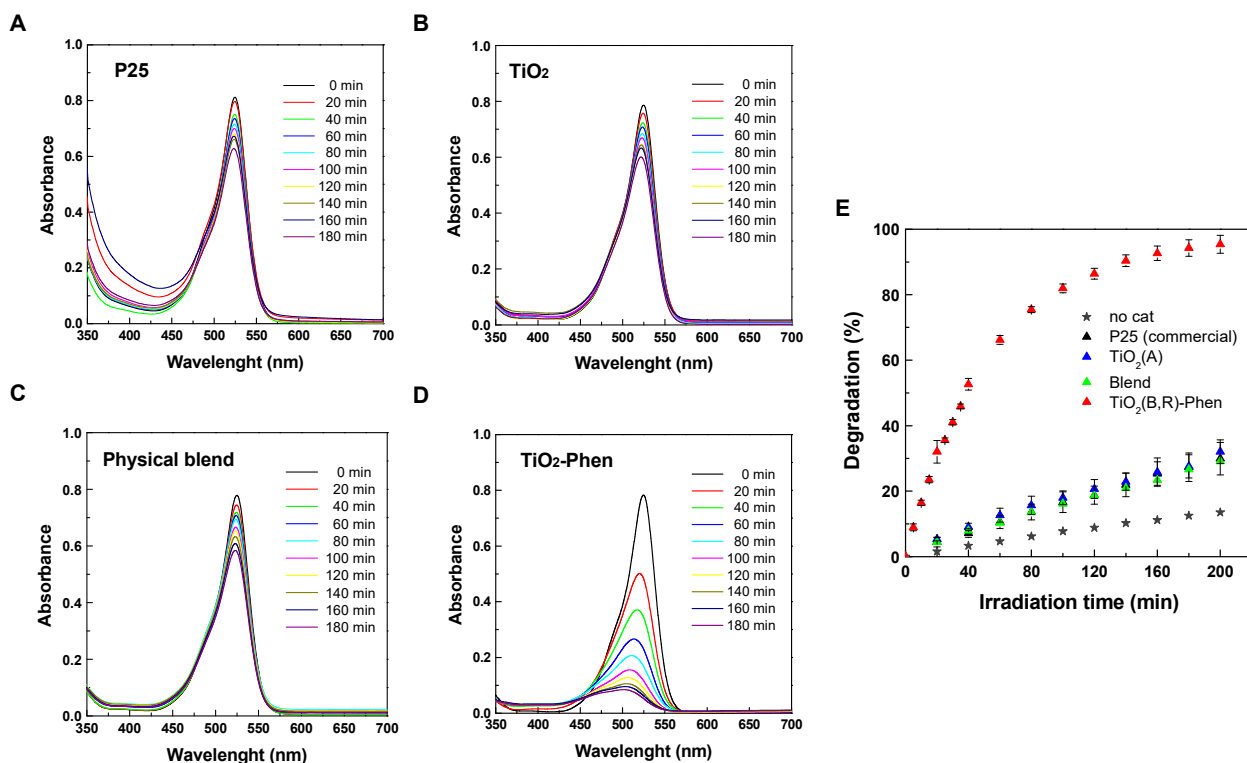
Figure S10. UV-vis absorption spectra of the degradation reaction of Rh6G at different times under visible light irradiation using as photocatalysts: (**A**) the commercial P25, (**B**) the unmodified $TiO_2(A)$ (crystallization time 36 h), (**C**) a physical blend of $TiO_2(A)$ with 12 wt% Phen, and (**D**) the hybrid $TiO_2(B,R)$-Phen (crystallization time 36 h). (**E**) Degree of conversion as a function of the irradiation time. Experiments were carried out under identical irradiation conditions, using 40 mg of photocatalysts and 100 ml of 1×10^{-5} M aqueous Rh6G solutions.
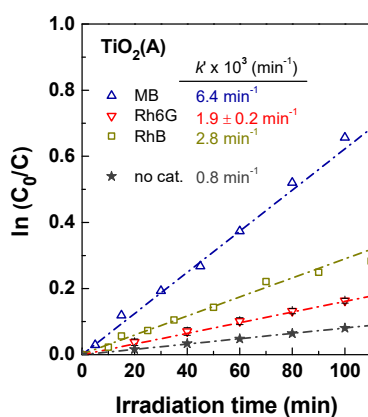
Figure S11. Photocatalytic activity of control $TiO_2(A)$ in the degradation reaction of Rh6G, RhB and MB: plots of ln (C_0/C) as a function of the irradiation time (symbols) and their corresponding linear fits (dashed lines). Inset shows the apparent constant rate ($k' \times 10^{-3}$, min^{-1}) for each degradation reaction as well as for the experiment carried out in absence of catalyst (star grey symbols). Experiments were carried out under identical irradiation conditions, using 40 mg of photocatalysts and 100 ml of 1×10^{-5} M aqueous dye solutions.
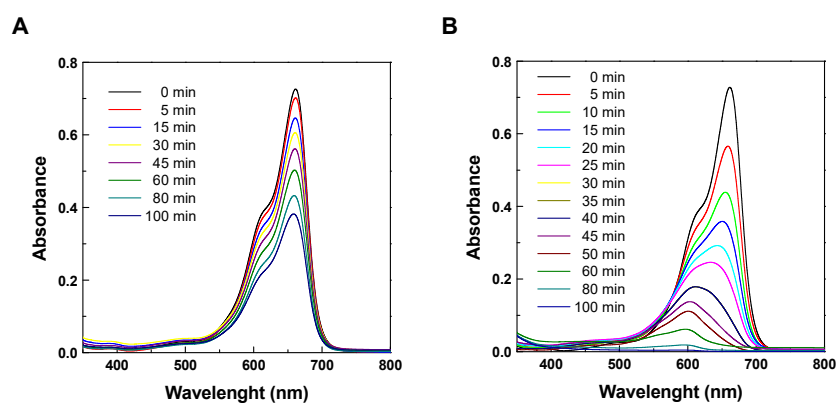
Figure S12. UV-vis absorption spectra of MB at different times of visible irradiation using as photocatalysts: (**A**) $TiO_2(A)$, and (**B**) $TiO_2(B,R)$-Phen. Both samples were crystallized at 100 ºC during 36 h. Experiments were carried out under identical irradiation conditions, using 40 mg of photocatalysts and 100 ml of 1×10^{-5} M aqueous MB solutions.
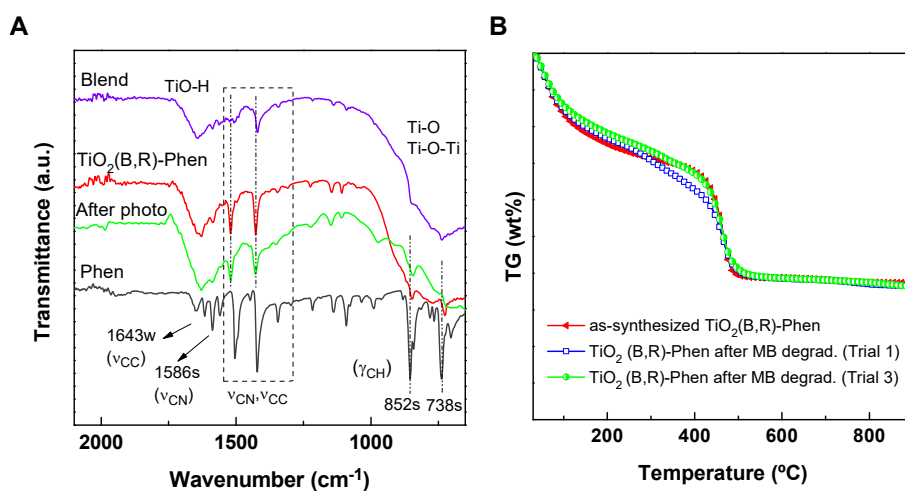
Figure S13. FTIR spectra (**A**) and TG curves (**B**) of the hybrid $TiO_2(B,R)$-Phen before –$TiO_2(B,R)$-Phen– and after the degradation reaction of MB (1×10^{-5} M, 100 ml) under visible light irradiation. FTIR spectra of the phenanthroline alone –Phen–, and physically blended with $TiO_2(A)$ (12 wt% Phen) –Blend– have been included for comparison purposes.
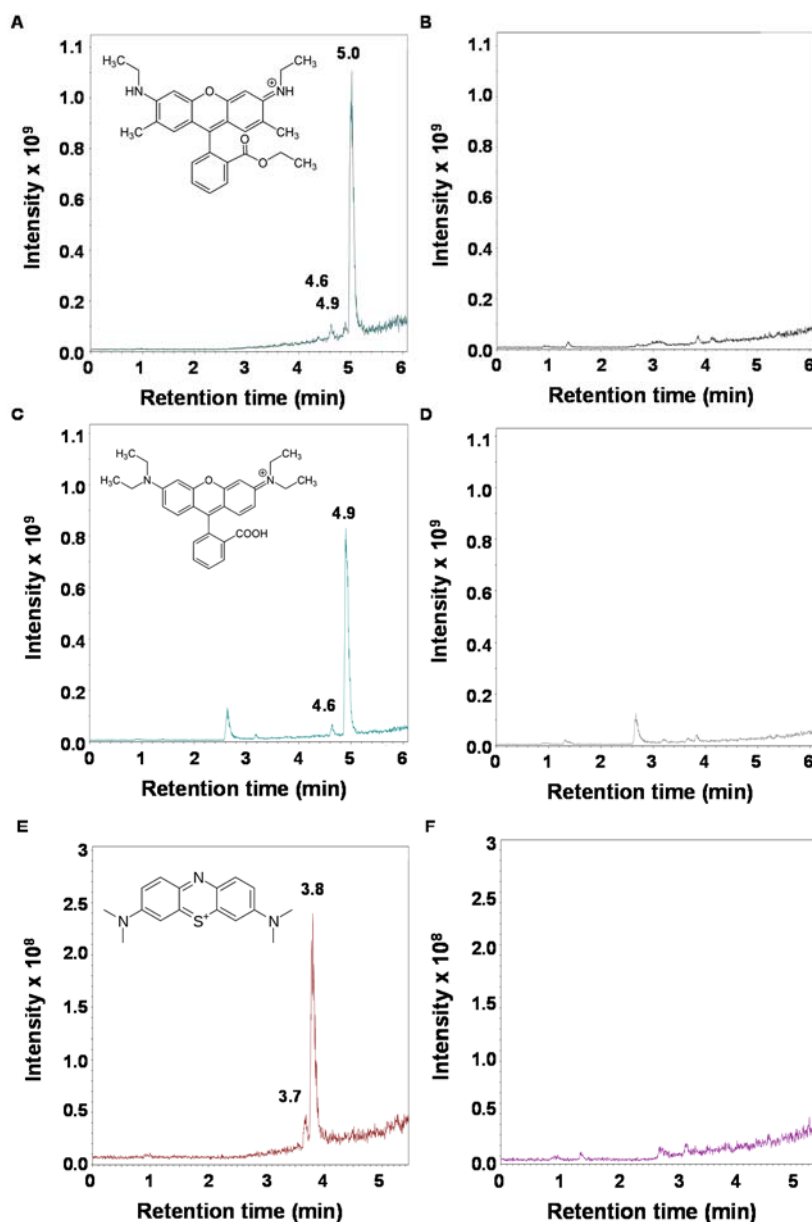
Figure S14. The total ion chromatogram (TIC) of Rh6G (top), RhB (middle), and MB (bottom) solutions before (left) and after (right) the photocatalytic degradation processes: (**A**) control Rh6G solution (1x10^{-5} M), (**B**) solution after the 4th degradation cycle of Rh6G, (**C**) control RhB solution (1x10^{-5} M), (**D**) solution after the RhB photocatalytic reaction, (**E**) control MB solution (1x10^{-5} M), and (**F**) solution after the MB photocatalytic process.

A   **B**
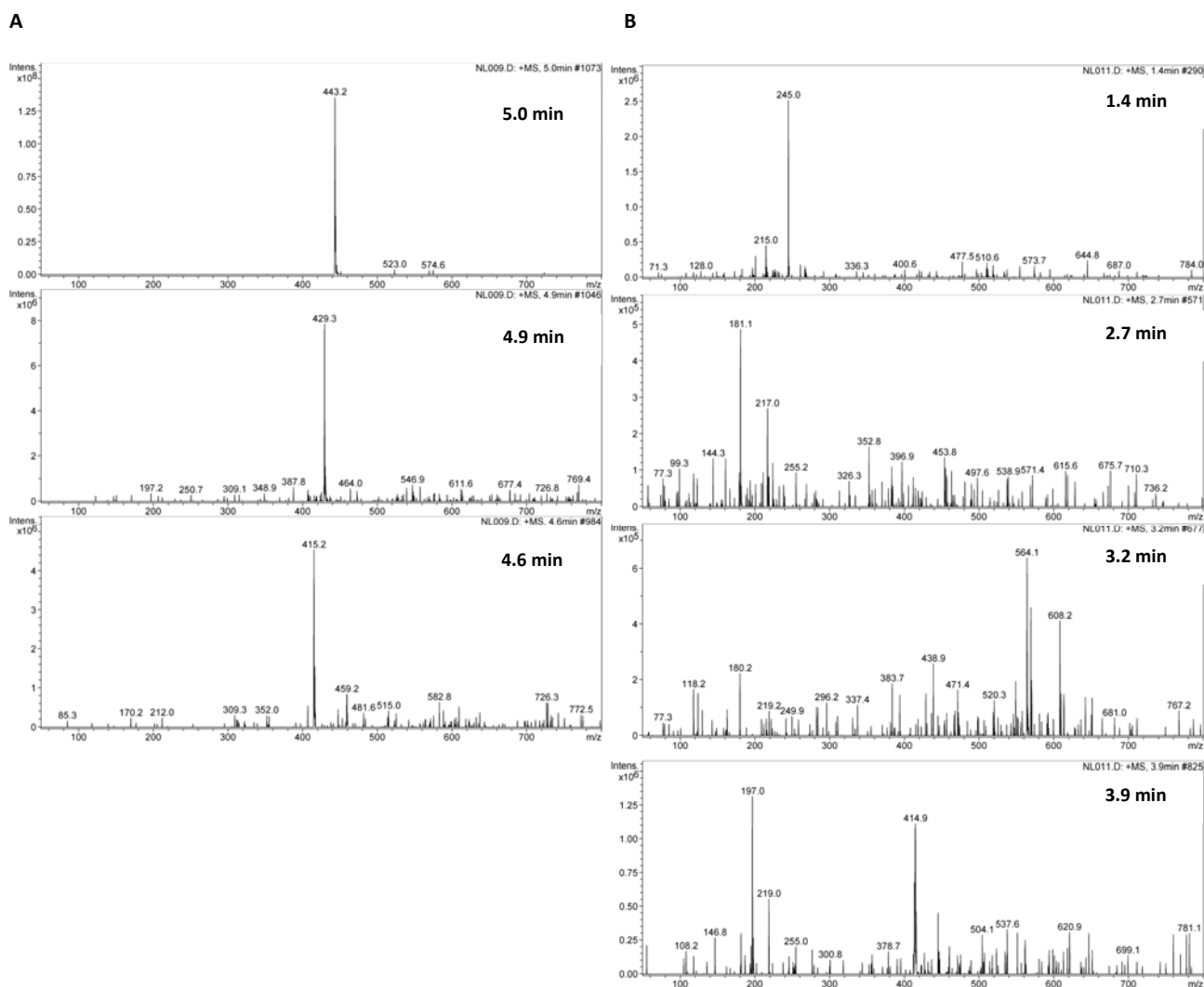
Figure S15. The EIS/MS spectra corresponding to the peaks appearing at the different retention times in the TIC chromatogram: (**A**) a control Rh6G solution (1x10^{-5} M), and (**B**) the treated solution after the fourth cycle of Rh6G degradation (Figure 8A of the main paper).
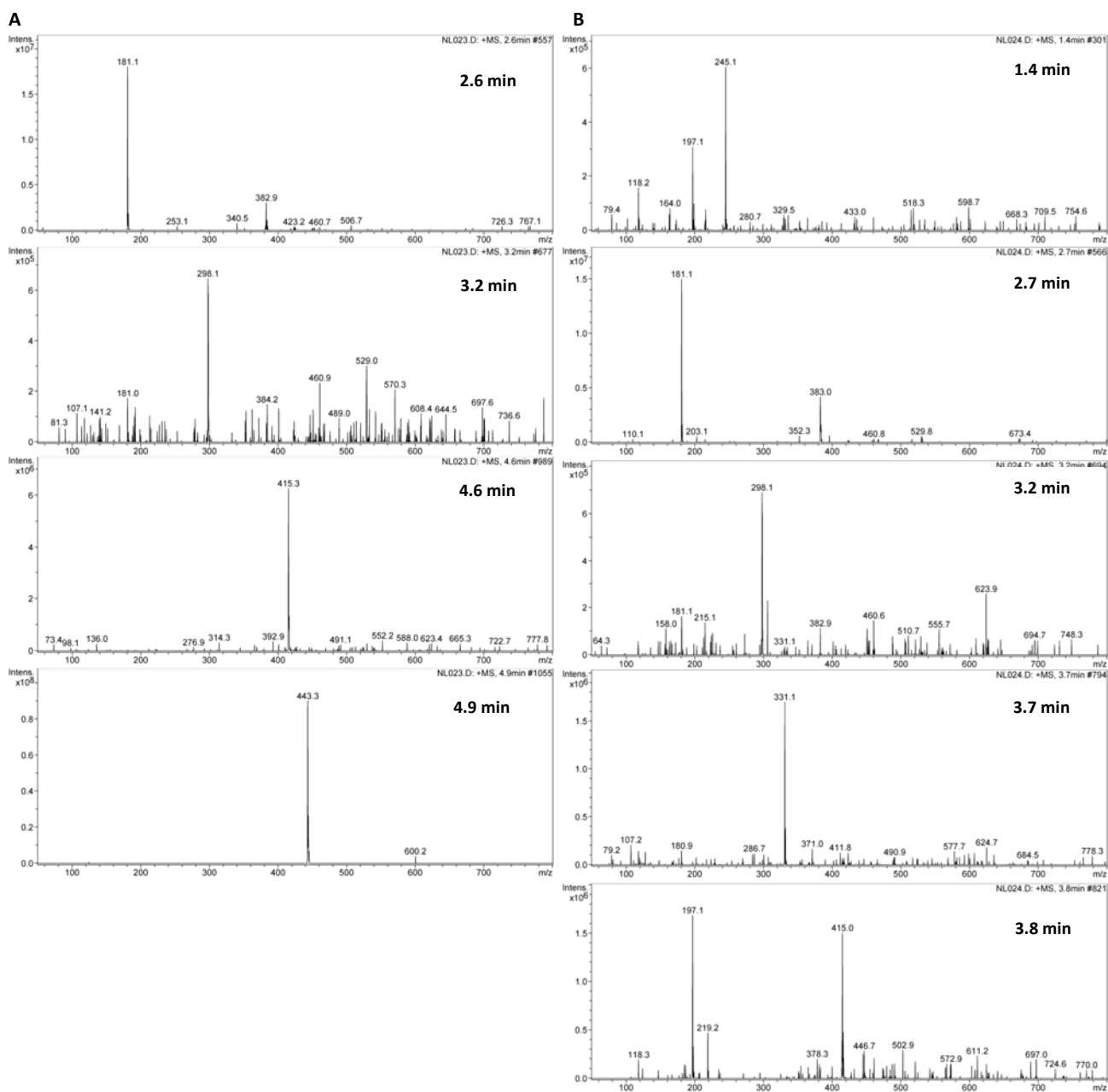
Figure S16. The EIS/MS spectra corresponding to the peaks appearing at the different retention times in the TIC chromatogram of: (**A**) a control RhB solution (1×10^{-5} M), and (**B**) the treated solution after 130 min of reaction time.

A

B
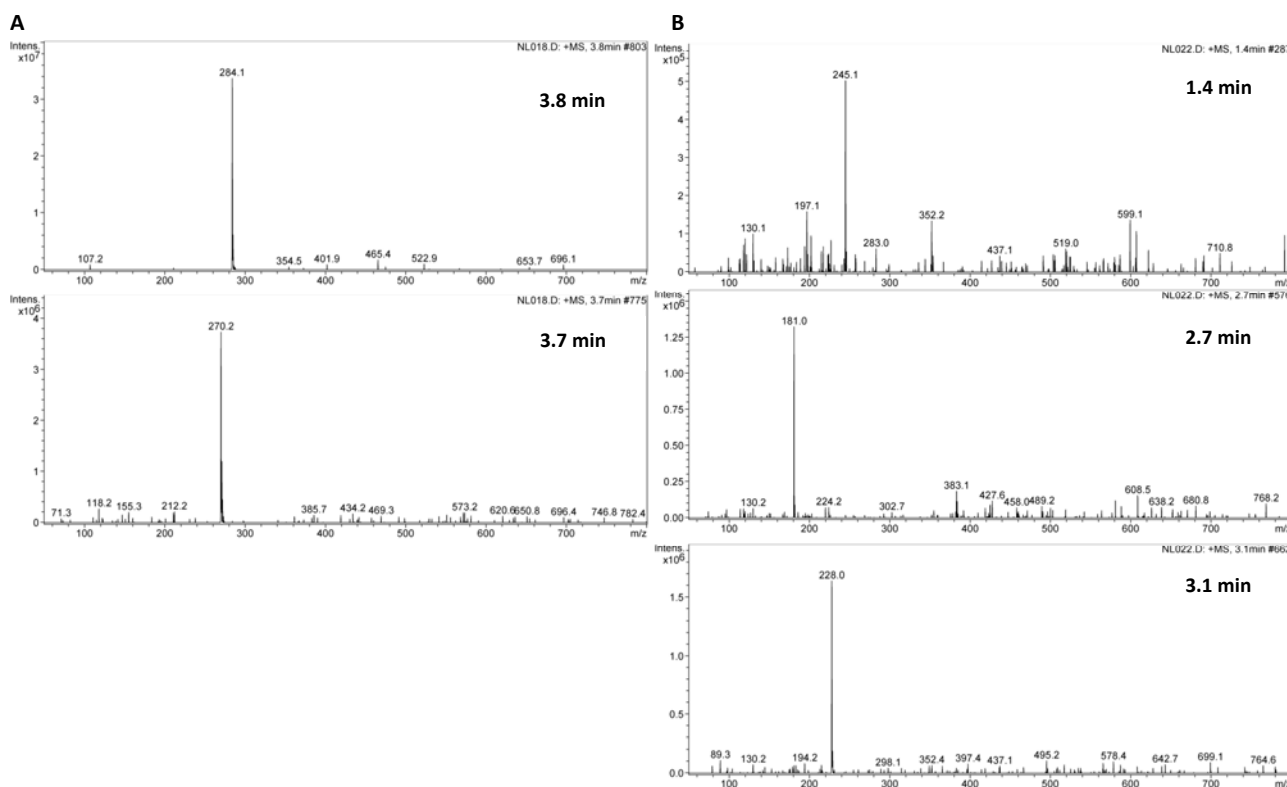
Figure S17. The EIS/MS spectra corresponding to the peaks appearing at the different retention times in the TIC chromatogram of: (**A**) a control MB solution (1×10^{-5} M), and (**B**) the treated solution after 100 min of photocatalytic reaction (Figure 7 of the main paper).

2.7 Electrical Characterization
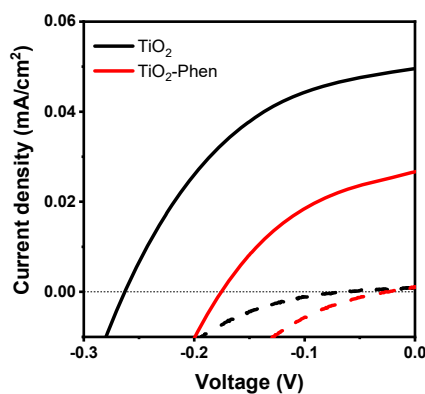
Figure S18. J-V curves for electrochemical cells prepared with TiO_2(A) (black) and TiO_2(B,R)-Phen hybrid (red) nanoparticles, at 1 sun (solid line) and dark (dashed line) conditions.
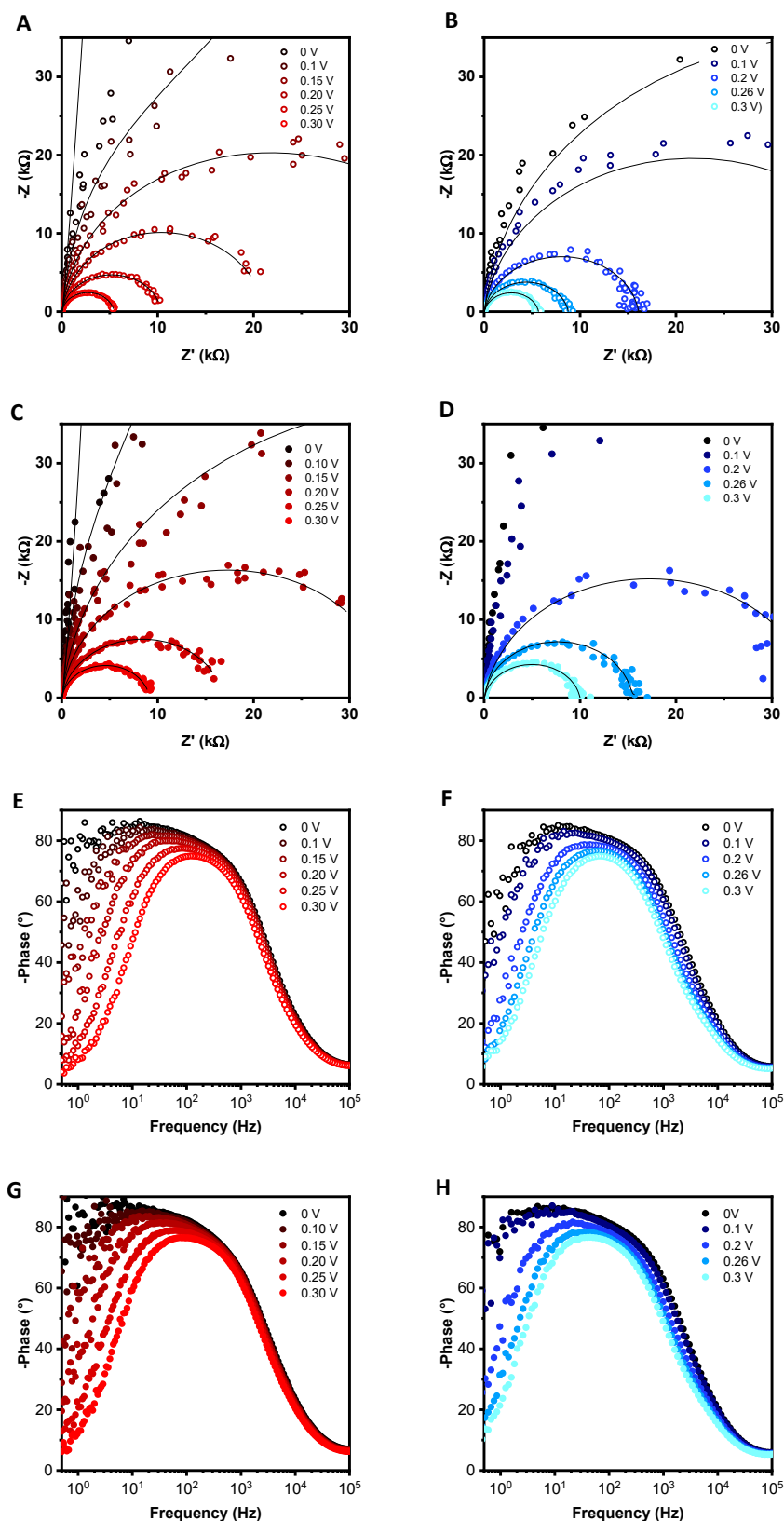
Figure S19. Nyquist (**A-D**) and Bode (**E-H**) plots and for electrochemical cells prepared with TiO$_2$(A) (blue) and TiO$_2$(B,R)-Phen hybrid (red) nanoparticles at 1 sun (open circle) and dark (solid circle) conditions.
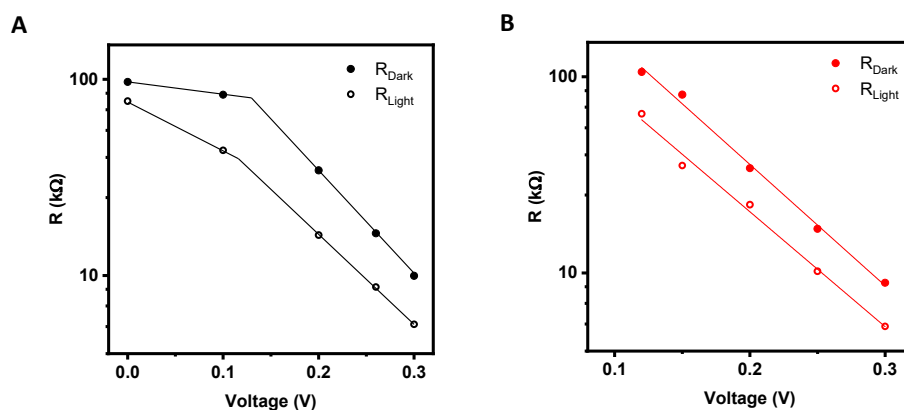
Figure S20. Electrode resistances at different applied bias for electrochemical cells prepared with $TiO_2(A)$ (**A**) and $TiO_2(B,R)$-Phen hybrid (**B**) nanoparticles, at 1 sun (open circle) and dark (solid circle) conditions.

References

1   C. C. Chusuei, M. A. Brookshier, D. W. Goodman, C. C. Chusuei, and M. A. Brookshier and D. W. Goodman*, Correlation of relative X-ray photoelectron spectroscopy shake-up intensity with CuO particle size, *Langmuir*, 1999, **15**, 2806–2808.

2   A. A. Gribb and J. F. Banfield, Particle size effects on transformation kinetics and phase stability in nanocrystalline TiO2, *Am. Mineral.*, 1997, **82**, 717–728.

3   H. Zhang and J. F. Banfield, Understanding polymorphic phase transformation behavior during growth of nanocrystalline aggregates: Insights from TiO2, *J. Phys. Chem. B*, 2000, **104**, 3481–3487.

4   K. Maeda, T. Takata, M. Hara, N. Saito, Y. Inoue, H. Kobayashi and K. Domen, GaN:ZnO solid solution as a photocatalyst for visible-light-driven overall water splitting, *J. Am. Chem. Soc.*, 2005, **127**, 8286–8287.

5   M. Rico-Santacruz, Á. E. Sepúlveda, C. Ezquerro, E. Serrano, E. Lalinde, J. R. Berenguer and J. García-Martínez, Bottom-up construction of highly photoactive dye-sensitized titania using Ru(II) and Ir(III) complexes as building blocks, *Appl. Catal. B Environ.*, 2017, **200**, 93–105.

6   C. A. Parker and C. G. Hatchard, in *Journal of Physical Chemistry*, American Chemical Society, 1959, vol. 63, pp. 22–26.

7   C. G. H. Atchard, A new sensitive chemical actinometer - II. Potassium ferrioxalate as a standard chemical actinometer, *Proc. R. Soc. London. Ser. A. Math. Phys. Sci.*, 1956, **235**, 518–536.

8   L. Sun and J. R. Bolton, Determination of the quantum yield for the photochemical generation of hydroxyl radicals in TiO2 suspensions, *J. Phys. Chem.*, 1996, **100**, 4127–4134.

9   H. Kisch and D. Bahnemann, *J. Phys. Chem. Lett.*, 2015, 6, 1907–1910.

10   J. Jiménez-López, N. Linares, E. Serrano and J. García-Martínez, Visible-Light-Activated Black Organotitanias: How Synthetic Conditions Influence Their Structure and Photocatalytic Activity, *Chempluschem*, 2018, **83**, 390–400.